J Biomol NMR (2013) 56:169–182
DOI 10.1007/s10858-013-9733-y

ARTICLE

Accurate measurements of the effects of deuteration at backbone amide positions on the chemical shifts of ^{15}N, $^{13}C_\alpha$, $^{13}C_\beta$, ^{13}CO and $^{1}H_\alpha$ nuclei in proteins

Daoning Zhang · Vitali Tugarinov

Received: 11 March 2013 / Accepted: 18 April 2013 / Published online: 24 April 2013

Abstract An approach towards accurate NMR measurements of deuterium isotope effects on the chemical shifts of all backbone nuclei in proteins (^{15}N, $^{13}C_\alpha$, ^{13}CO, $^{1}H_\alpha$) and $^{13}C_\beta$ nuclei arising from ^{1}H-to-D substitutions at amide nitrogen positions is described. Isolation of molecular species with a defined protonation/deuteration pattern at successive backbone nitrogen positions in the polypeptide chain allows quantifying all deuterium isotope shifts of these nuclei from the first to the fourth order. Some of the deuterium isotope shifts measured in the proteins ubiquitin and GB1 can be interpreted in terms of backbone geometry via empirical relationships describing their dependence on (φ; ψ) backbone dihedral angles. Because of their relatively large variability and notable dependence on the protein secondary structure, the two- and three-bond $^{13}C_\alpha$ isotope shifts, $^{2}\Delta C_\alpha(N_iD)$ and $^{3}\Delta C_\alpha(N_{i+1}D)$, and three-bond $^{13}C_\beta$ isotope shifts, $^{3}\Delta C_\beta(N_iD)$, are useful reporters of the local geometry of the protein backbone.

Keywords Deuterium isotope shifts · Chemical shifts · Deuteration · Protein backbone geometry · Isotope filtering

Introduction

The importance of deuterium isotope shifts (Hansen 1983, 1988, 2000), the secondary changes in isotropic chemical shielding of nuclei removed by one or more bonds away from the site of a proton-to-deuterium (^{1}H-to-D) substitution has been recognized more than three decades ago—initially, in small organic compounds (Anet and Dekmezian 1979; Aydin and Günther 1981; Ernst et al. 1982; Jameson 1996; Majerski et al. 1985; Reuben 1985) and, later, in bio-molecules (Feeney et al. 1974; Hawkes et al. 1978; Henry et al. 1987; Kainosho et al. 1987; Otter et al. 1990; Ottiger and Bax 1997; Tüchsen and Hansen 1991). Most of the quantitative NMR studies of deuterium isotope effects in peptides and proteins concentrated on the effects of ^{1}H-to-D substitutions at exchangeable sites of amides, Tyr hydroxyl or Cys sulfhydryl groups giving rise to the isotope shifts of carbonyl carbons (Feeney et al. 1974; Hawkes et al. 1978; Henry et al. 1987; Kainosho et al. 1987; Otter et al. 1990; Tüchsen and Hansen 1991), $^{13}C_\alpha$ and $^{13}C_\beta$ nuclei (Meissner et al. 1998; Meissner and Sørensen 1998; Ottiger and Bax 1997) and, recently, Tyr $^{13}C_\zeta$ (Takeda et al. 2009) and Cys $^{13}C_\beta$ sites (Takeda et al. 2010). The effects of hydrogen-bonding on one-bond isotope shifts of backbone ^{15}N nuclei (Abildgaard et al. 2009; Jaravine et al. 2004), ^{15}N in NH_2 groups of asparagine and glutamine side-chains (Liu et al. 2008) and $^{15}N/^{1}H$ nuclei in NH_3 groups of lysines (Tomlinson et al. 2009) have been reported.

Unlike the effects of ^{1}H-to-D substitutions at exchangeable sites that tend to be isolated in the polypeptide chain (separated from each other by multiple bonds), the measured isotope effects arising from ^{1}H-to-D replacements at aliphatic carbon positions are usually cumulative as all these sites are commonly deuterated simultaneously and the effects of multiple ^{1}H-to-D replacements are additive (Hansen 2000; Jameson 1996). Therefore, it is often difficult to disentangle the contributions of multiple replacements to the total isotope shift of a

Electronic supplementary material The online version of this article (doi:10.1007/s10858-013-9733-y) contains supplementary material, which is available to authorized users.

D. Zhang · V. Tugarinov (✉)
Department of Chemistry and Biochemistry, University of Maryland, Biomolecular Sci. Bldg./CBSO, College Park, MD 20742, USA
e-mail: vitali@umd.edu

particular nucleus. Although these deuterium isotope shifts are frequently viewed as a nuisance because they complicate assignments of protein resonances (Garrett et al. 1997; Sheppard et al. 2009a, b; Venters et al. 1996) and (in the case of partial deuteration) also broaden ^{13}C lines, the knowledge of their accurate values is important for better understanding of their physical and structural origins. These isotope effects have been quantified on a number of occasions from comparisons of chemical shifts in fully protonated and fully deuterated protein molecules (Gardner and Kay 1998; Gardner et al. 1997; Garrett et al. 1997; Venters et al. 1996). Earlier, LeMaster et al. (1994) used differential isotope shifts of $^{13}C_\alpha$ nuclei in glycines to establish conformational preferences of glycine residues in proteins. Recently, Bax and co-workers have suggested an approach for 'de-convolution' of multiple contributions to deuterium isotope effects on the chemical shifts of all backbone nuclei arising from the deuteration of non-exchangeable aliphatic sites of an intrinsically disordered protein α-synuclein (Maltsev et al. 2012).

In structured proteins, deuterium isotope shifts of either variety have been demonstrated to be useful reporters of local backbone geometry (LeMaster et al. 1994; Ottiger and Bax 1997; Sun and Tugarinov 2012); hydrogen exchange rates (Takeda et al. 2010) and hydrogen bonding (Jaravine et al. 2004; Tüchsen and Hansen 1991). Here, we describe the measurements of deuterium isotope effects on the chemical shifts of ^{15}N, $^{13}C_\alpha$, ^{13}CO, $^{13}C_\beta$ and $^{1}H_\alpha$ nuclei resulting from $^{1}H_N \rightarrow D_N$ substitutions at backbone amide positions using an extension of the approach we recently developed for quantification of deuterium isotope effects on the chemical shifts of ^{15}N, ^{13}CO, $^{13}C_\alpha$ and $^{1}H_N$ nuclei arising from ^{1}H-to-D substitutions at aliphatic carbon sites (Sun and Tugarinov 2012). Isolation of molecular species with a defined protonation/deuteration pattern at successive backbone nitrogen positions in the polypeptide chain allowed us to accurately measure all deuterium isotope shifts of nuclei removed from one to four bonds away from the sites of the ^{1}H-to-D replacement. When possible, the isotope shifts measured in the proteins ubiquitin and GB1 are interpreted in terms of backbone geometry via empirical Karplus-type relationships describing their dependence on the backbone φ and ψ torsion angles.

Materials and methods

NMR samples

The samples of two proteins have been used in this work: (1) wild-type human ubiquitin, and (2) immunoglobulin-binding domain of protein G from *Staphylococcus aureus*, GB1. Both proteins were [U–^{15}N; ^{13}C]-labeled and fully protonated (obtained using [U–^{13}C]-glucose as a carbon source in H_2O minimal media). The sample of GB1 has been obtained using a co-expression vector where the sequence of GB1 serves as a removable tag, resulting in the addition of seven residues (–Ser–Ser–Gly–Leu–Val–Pro–Arg) to the C-terminus of the protein (Sheppard et al. 2009c). The sample of ubiquitin was 1.5 mM in protein concentration and dissolved in a 20 mM sodium phosphate buffer (pH 4.7) containing 0.03 % NaN_3. The sample of GB1 was 1.1 mM in protein concentration and dissolved in a 25 mM sodium phosphate buffer (pH 6.0) containing 50 mM NaCl and 0.03 % NaN_3. NMR samples of both proteins were incubated in buffering solutions containing a 50 % D_2O/50 % H_2O mixture to ensure ~50 % deuteration at exchangeable amide positions.

Experimental NMR details

Figure 1 shows the two-dimensional (2D) *intra*-HA[CA/CO/N/CB] pulse-scheme that has been designed for precision measurements of deuterium isotope effects arising from proton-to-deuterium substitution at amide positions on the chemical shifts of ^{15}N, $^{13}C_\alpha$, ^{13}CO, $^{13}C_\beta$ and $^{1}H_\alpha$ nuclei of proteins. Four types of 2D data sets are recorded—(1) [$^{1}H_\alpha$–$^{13}C_\alpha$] with acquisition times [t_2, t_1], (2) [$^{1}H_\alpha$–^{13}CO] with acquisition times [t_2, t_1'], (3) [$^{1}H_\alpha$–^{15}N] with acquisition times [t_2, t_1''] (inset '^{15}N' in Fig. 1), and (4) [$^{1}H_\alpha$–$^{13}C_\beta$] with acquisition times [t_2, t_1'''] (inset '$^{13}C_\beta$' in Fig. 1)—each with different phase-cycling schemes leading to individual sub-spectra that isolate the molecular species with each of the four deuteration patterns shown for a fragment of the polypeptide chain in Fig. 2 (see "Results and discussion" for details). Two successive bilinear rotation decoupling (BIRD) filtering elements (Briand and Sørensen 1997; Garbow et al. 1982) (labeled $\boldsymbol{F_1}$ and $\boldsymbol{F_2}$ in Fig. 1) ensure that correlations corresponding to only one type of isotopic species (with a certain protonation/deuteration pattern at two successive nitrogen sites; Fig. 2) is obtained in a single sub-spectrum. The comparison of chemical shifts of the same correlation in the four different sub-spectra provides deuterium isotope shifts. Excellent water suppression in the scheme of Fig. 1 has been achieved via application of high-power ^{1}H purge pulses followed by a (gradient—^{1}H 90° pulse—gradient) element (Fig. 1).

NMR measurements and data analysis

All NMR measurements were performed on a 600 MHz Bruker Advance III spectrometer equipped with a room temperature triple-resonance *z*-gradient probe operating at 30 °C. 2D NMR data sets recorded with the pulse scheme of Fig. 1, comprised [512; 82]* (complex) points in the

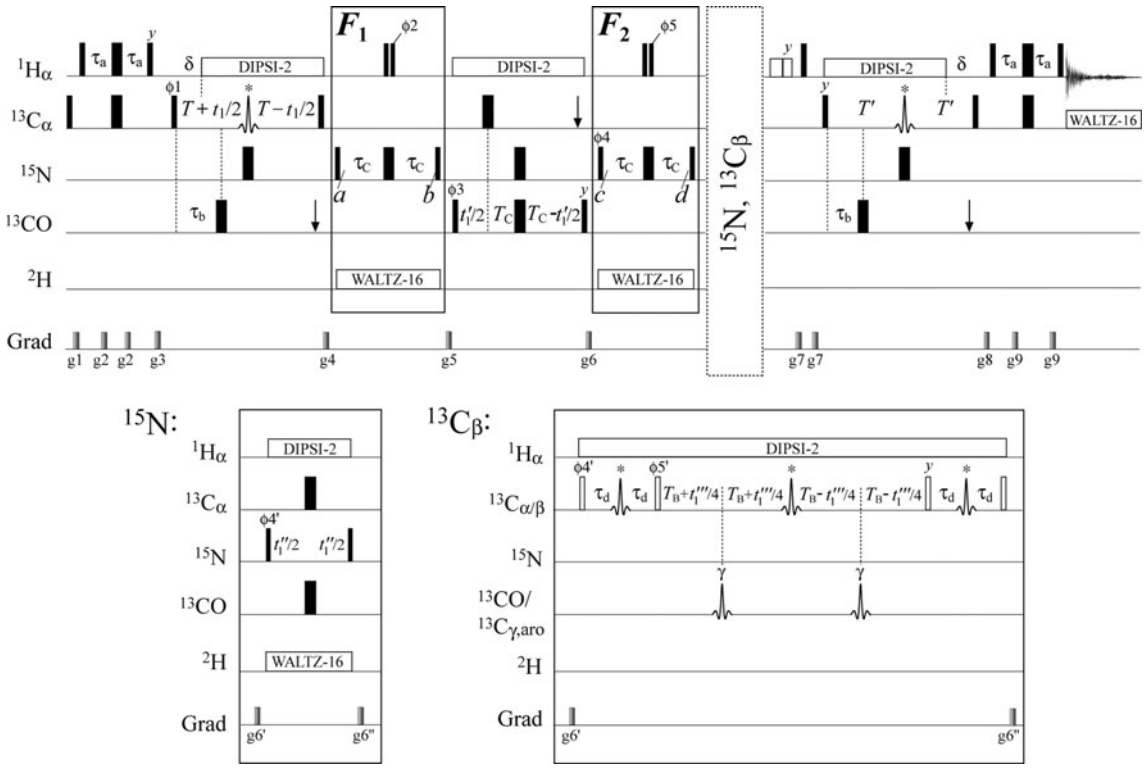

Fig. 1 2D *intra*-HA[CA/CO/N/CB] pulse-scheme for measurements of deuterium isotope effects arising from deuteration of amide positions on the chemical shifts of ^{15}N, $^{13}C_\alpha$, ^{13}CO, $^{13}C_\beta$ and $^{1}H_\alpha$ nuclei of proteins. All narrow(wide) *rectangular pulses* are applied with the flip angles of 90°(180°) along the *x*-axis unless indicated otherwise. The $^{1}H(^{2}H; ^{15}N)$ carriers are positioned at 4.7(4.5; 119) ppm. The ^{13}C carrier is placed at 57 ppm, switched to 176 ppm before the first 90° ^{13}CO pulse (after the gradient g5), and returned to 57 ppm after the gradient g6. $^{13}C_\alpha$ WALTZ-16 decoupling (Shaka et al. 1983) during acquisition is achieved using a 2.5 kHz field, while ^{2}H WALTZ-16 decoupling uses a 0.9 kHz field. ^{1}H DIPSI-2 decoupling (Shaka et al. 1988) is applied with a 7.5 kHz field. All ^{1}H and ^{15}N pulses are applied with maximum available power, while the two consecutive ^{1}H pulses shown with *open rectangles* (preceding g7) are 9-ms and 6-ms long and use a 12 kHz power. All rectangular 90°(180°) $^{13}C_\alpha$ and ^{13}CO pulses are applied with a field strength of $\Delta/\sqrt{15}$ $(\Delta/\sqrt{3})$ where Δ is the difference (in Hz) between $^{13}C_\alpha$ and ^{13}CO chemical shifts (Kay et al. 1990). *Vertical arrows* at the end of $2T$, $2T_C$ and $2T'$ periods indicate the positions of the $^{13}CO/^{13}C_\alpha$ Bloch-Siegert shift compensation pulses. ^{13}C shaped pulses labeled with *asterisks* are 340-μs RE-BURP pulses (Geen and Freeman 1991) centered at 40 ppm by phase modulation of the carrier (Boyd and Soffe 1989; Patt 1992) and cover the range of all aliphatic ^{13}C chemical shifts. The ^{13}C shaped pulses labeled with 'γ' are 350-μs RE-BURP pulses centered at 150 ppm and cover the range of chemical shifts from ^{13}CO nuclei of Asn and Asp side-chains to $^{13}C^{\gamma}$ nuclei of aromatic residues. $^{13}C_\beta$-pulses shown with *open rectangles* are centered at 43 ppm. Delays are: $\tau_a = 1.75$ ms; $\tau_b = 4.5$ ms; $\tau_C = 5.4$ ms; $\tau_d = 7$ ms; $T = 27.5$ ms; $T_C = 16.5$ ms; $T' = 14$ ms; $T_B = 7$ ms; $\delta = 3.5$ ms. The phase-cycle is: $\phi1 = x, -x$; $\phi2 = 16(x), 16(-x)$; $\phi3 = 2(x), 2(-x)$; $\phi4 = 4(x), 4(-x)$ if the '^{15}N' or '$^{13}C_\beta$' insets are not used and $\phi4 = x$ for insets '^{15}N' or '$^{13}C_\beta$'; $\phi4' = 4(x), 4(-x)$; $\phi5 = 8(x), 8(-x)$; $\phi5' = y$; rec. $= 4(x, -x, -x, x, -x, x, x, -x)$ for selection of $D_{N,i}D_{N,i+1}$ species (Fig. 2a), rec. $= (x, -x, -x, x, -x, x, x, -x)$, $(-x, x, x, -x, x, -x, -x, x)$, $(-x, x, x, -x, x, -x, -x, x)$, $(x, -x, -x, x, -x, x, x, -x)$ for $H_{N,i}D_{N,i+1}$ (Fig. 2b) selection, rec. $= 2(x, -x, -x, x, -x, x, x, -x)$, $2(-x, x, x, -x, x, -x, -x, x)$ for $D_{N,i}H_{N,i+1}$ (Fig. 2c) selection, and rec. $= 2(x, -x, -x, x, -x, x, x, -x, -x, x, x, -x, -x, x, x, -x)$ for selection of $H_{N,i}H_{N,i+1}$ (Fig. 2d). Quadrature in $t_1(t_1'; t_1'')$ is achieved via STATES-TPPI (Marion et al. 1989) of phases $\phi1(\phi3; \phi4')$, while quadrature in t_1''' uses STATES-TPPI of $\phi4'$ and $\phi5'$. Durations and strengths of pulsed-field gradients in units of (ms;G/cm) are: g1 = (1; 20); g2 = (0.3; 5); g3 = (1.5; 20); g4 = (0.6; 8); g5 = (0.8; 10); g6 = (0.7; 8); g6′ = (0.6; 10); g6″ = (0.8; 15); g7 = (1; 15); g8 = (0.8; 8); g9 = (0.4; 12)

corresponding dimensions of the $[^{1}H_\alpha; ^{13}C_\alpha]$ correlation maps, [512; 42]* points in the corresponding dimensions of the $[^{1}H_\alpha; ^{13}CO]$ maps, [512; 64]* points in the corresponding dimensions of the $[^{1}H_\alpha; ^{15}N]$ maps, and [512; 50]* points in the corresponding dimensions of the $[^{1}H_\alpha; ^{13}C_\beta]$ maps, with the respective acquisition times of [64; 55] ms, [64; 33] ms, [64; 53] ms and [64; 28] ms. Typically, a recovery delay of 1.4 s was used along with 128 or 256 scans/FID giving rise to net acquisition times of ~9 h per each 2D experiment. Longer acquisition times were necessary for the recording of 2D $[^{1}H_\alpha; ^{13}C_\beta]$ correlation maps: 512 scans per fid and a 1.0 s recovery delay resulted in the net acquisition times of ~16 h per 2D spectrum. The 3D HACBN(H/D) data sets have been recorded using minor modifications of the second variant of the pulse scheme described by (Meissner and Sørensen 1998) (see Figure 1b in Meissner and Sørensen 1998) with net acquisition times of ~24 h per 3D dataset.

All NMR spectra were processed and analyzed using the NMRPipe/NMRDraw suite of programs (Delaglio et al.

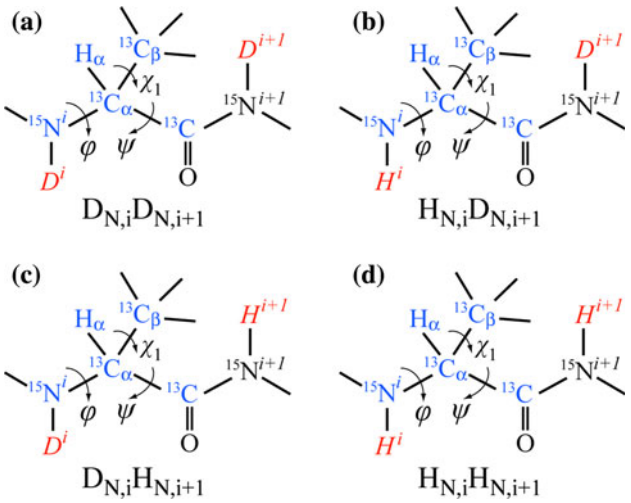

Fig. 2 Schematic representation of a fragment of polypeptide chain in various states of protonation/deuteration at backbone amide positions. The nuclei whose isotope shifts have been measured in this work are shown in *blue*, while the sites of proton-to-deuterium substitution are indicated in *red*. Torsion angles of residue *i* are indicated with *arrows*. Double-filtering achieved by the elements $\boldsymbol{F_1}$ and $\boldsymbol{F_2}$ of the scheme in Fig. 1, ensures isolation of NMR signals corresponding to each type of isotopic species: **a** $D_{N,i}D_{N,i+1}$; **b** $H_{N,i}D_{N,i+1}$; **c** $D_{N,i}H_{N,i+1}$, and **d** $H_{N,i}H_{N,i+1}$

1995). All the data sets were linear predicted to 3/2 of their original size via mirror-image (Zhu and Bax 1990) or complex forward–backward (Zhu and Bax 1992) linear prediction algorithms. Deuterium isotope effects on the chemical shifts of backbone nucleus *X* resulting from the substitution of a proton nucleus for deuterium at amide site *i*, ($^1H_{N,i} \rightarrow D_{N,i}$) are defined as $^n\Delta X(N_iD) = \delta X(H_{N,i}) - \delta X(D_{N,i})$, where *n* is the number of bonds between the observed nucleus *X* and the position of the isotopic H → D substitution (Hansen 1988, 2000; Ottiger and Bax 1997). Each of the isotope shift measurements (except for the $^{13}C_\beta$ shifts) has been performed twice, and the errors in the measurements estimated from pair-wise r.m.s.d. between duplicate experiments. Random uncertainties estimated in this manner and averaged for ubiquitin and GB1 are: 7.6(4.0) ppb for the $^1\Delta N(N_iD)(^4\Delta N(N_{i+1}D))$ isotope shifts, 2.1(1.8) ppb for $^2\Delta C_\alpha(N_iD)(^3\Delta C_\alpha(N_{i+1}D))$ shifts, and 2.6(2.4) ppb for $^2\Delta C'(N_{i+1}D)(^3\Delta C'(N_iD))$ shifts. Random errors in the measurements of $^3\Delta C_\beta(N_iD)$ and $^4\Delta C_\beta(N_{i+1}D)$ have been derived from the pair-wise r.m.s.d between the shifts obtained using the scheme of Fig. 1 and those measured from the 3D HACBN(H/D) datasets: 4.1 and 4.5 ppb, respectively.

Best fits between the observed isotope shifts and backbone torsion angles were calculated via the least squares minimization using Matlab (MathWorks Inc., MA, USA). Dihedral angles (φ; ψ) used for the derivation of empirical relationships have been obtained from the 1.8 Å crystal structure of ubiquitin [pdb access code—1ubq (Vijay-Kumar et al. 1987)] and the 1.0 Å crystal structure of GB1 [pdb code—2qmt (Frericks-Schmidt et al. 2007)]. None of the conclusions of this study would change significantly if the dihedral angles from the X-ray structures of chemically synthesized ubiquitin (pdb code—1ubi) (Alexeev et al. 1994; Ramage et al. 1994) or the 2.1 Å structure of GB1 from streptococcal protein G [pdb access code—1pga (Gallagher et al. 1994)] are considered instead. The pair-wise r.m.s.d. between the (φ; ψ) sets of angles in different structures of either protein is less than 5°—too small a difference to affect the parameterization of isotope effects via Karplus-type relationships.

Results and discussion

Experimental approach for accurate measurements of deuterium isotope shifts resulting from $^1H_N \rightarrow D_N$ substitution

Recently, we have developed an experimental NMR strategy for precise measurements of deuterium isotope effects on the chemical shifts of backbone nuclei in proteins (^{15}N, ^{13}CO, $^{13}C_\alpha$ and ^1HN) arising from ^1H-to-D substitutions at aliphatic carbons—primarily $^{13}C_\alpha$ positions. Isolation of molecular species with a defined protonation/deuteration pattern at successive carbon-α sites allowed distinguishing and accurately quantifying different isotope effects within the protein backbone. Here, we adapt this approach for the measurements of deuterium isotope effects on the chemical shifts of ^{15}N, $^{13}C_\alpha$, ^{13}CO, $^{13}C_\beta$ and $^1H_\alpha$ nuclei resulting from $^1H_N \rightarrow D_N$ substitutions at backbone amides. The *intra*-HA[CA/CO/N/CB] experiment (Fig. 1) employs two BIRD filtering elements (Briand and Sørensen 1997; Garbow et al. 1982) ($\boldsymbol{F_1}$ and $\boldsymbol{F_2}$) to obtain correlations of only one type of the four molecular isotopic species shown in Fig. 2. In the following, we succinctly describe how this is accomplished.

At time point *a* of the scheme (Fig. 1), the magnetization of interest is present in the form, $8C^\alpha_{z,i}CO_{z,i}N_{y,i+1}N_{y,i}$ (here and below we omit the trigonometric factors and all the terms that do not lead to observable magnetization in the end of the experiment), where $^{13}C_\alpha$ nuclei have evolved to the anti-phase state with respect to the nitrogen in the same residue (N_i) and the following residue (N_{i+1}), while the $^1J_{C\alpha-C\beta}$ couplings are refocused ($2T$ period $\approx 2/^1J_{C\alpha-C\beta}$). The molecular species having different isotopic content can be differentiated based on the evolution of $^1J_{N-H}$ couplings in ^{15}N–^1H spin-systems for a total period of $2\tau_C = 1/^1J_{N-H}$ and the absence of such evolution in ^{15}N–D groups—in the manner described earlier by Meissner and Sørensen (1998; Meissner et al. 1998). In the presence of $^1J_{N-H}$ evolution ($\phi 2 = x$), after the time-period

$2\tau_C$ in the first element $\boldsymbol{F_1}$ (time point *b*), the magnetization transforms as:

$$8C^{\alpha}_{z,i}CO_{z,i}N_{y,i+1}N_{y,i} \rightarrow \pm 8C^{\alpha}_{z,i}CO_{z,i}N_{y,i+1}N_{y,i} \quad (1)$$

where the isotopic species of $H_{N,i}H_{N,i+1}$ and $D_{N,i}D_{N,i+1}$ variety (Fig. 2) will retain their sign ('+'), while the signs of the species $H_{N,i}D_{N,i+1}$ and $D_{N,i}H_{N,i+1}$ will be inverted ('−'). The concomitant phase-cycling of ϕ2 (the phase of the second pulse of the pair of ^{1}H 90° pulses in the BIRD element $\boldsymbol{F_1}$; Fig. 1) and the receiver selects for either pair of molecular species. Subsequently, the magnetization is transformed to $4C^{\alpha}_{z,i}CO_{z,i}N_{y,i}$ via the evolution of $^1J_{CO-Ni+1}$ couplings during the time period $2T_C$ (time-point *c*). Again, in the presence of $^1J_{N-H}$ evolution ($\phi 5 = x$), after the $2\tau_C$ period (time point *d* in the second element $\boldsymbol{F_2}$; Fig. 1) this magnetization transforms as:

$$4C^{\alpha}_{z,i}CO_{z,i}N_{y,i} \rightarrow \pm 4C^{\alpha}_{z,i}CO_{z,i}N_{y,i} \quad (2)$$

where the species $D_{N,i}H_{N,i+1}$ and $D_{N,i}D_{N,i+1}$ will retain their sign ('+'), while the signs of their $H_{N,i}D_{N,i+1}$ and $H_{N,i}H_{N,i+1}$ counterparts will be inverted ('−'). The phase-cycling of ϕ5 (the phase of the second pulse of the pair of ^{1}H 90° pulses in the BIRD element $\boldsymbol{F_2}$; Fig. 1) and the receiver selects only a single type of isotopic species from each pair of species that had been selected earlier via the element $\boldsymbol{F_1}$. The advantage of this approach over the previously described 3D HACAN-/HACA(CO)N-based measurements of two- and three-bond $^{13}C_\alpha$ isotope shifts (Ottiger and Bax 1997), 2D HA(CA)CO-based measurements of two-bond ^{13}CO shifts (LiWang and Bax 1996) and 3D HACBN-based measurements of three- and four-bond $^{13}C_\beta$ shifts (Meissner and Sørensen 1998) lies primarily in the possibility of measuring the deuterium isotope effects on all the nuclei (^{15}N, $^{13}C_\alpha$, ^{13}CO, $^{13}C_\beta$ and $^1H_\alpha$) using essentially the same experimental scheme. Note that the correlations of the first residue (Met^1 in both proteins) and glycine residues are not observed in spectra acquired with the scheme of Fig. 1 because the delays δ are optimized for observation of methine groups. The use of shorter delays δ (~2.4 ms) would make observation of Gly $^{13}C_\alpha H_2$ groups possible at the expense of ~10 % reduction in sensitivity of all non-Gly correlations. This option has not been pursued here as Gly $^{13}C_\alpha$ magnetization would decay approximately twice faster due to the presence of two α protons (Sun et al. 2013). Examples of displacements in peak positions in the 2D *intra*-HA[CA/CO/N/CB] correlation maps arising from the isotope effects of the $^1H_N \rightarrow D_N$ substitutions are illustrated in Fig. 3. The differences in chemical shifts between protonated and deuterated molecular species defined in Fig. 2, are labeled with the corresponding isotope effect in each of the maps, with the black contours corresponding to the most deuterated isotopic forms, $D_{N,i}D_{N,i+1}$, in all the plots.

The selection of all the four isotopic species listed in Fig. 2 is not necessary for the measurement of each given isotope shift, i.e. the set of four sub-spectra is redundant for determination of all isotope shifts up to the fourth order. However, because many of the measured isotope effects

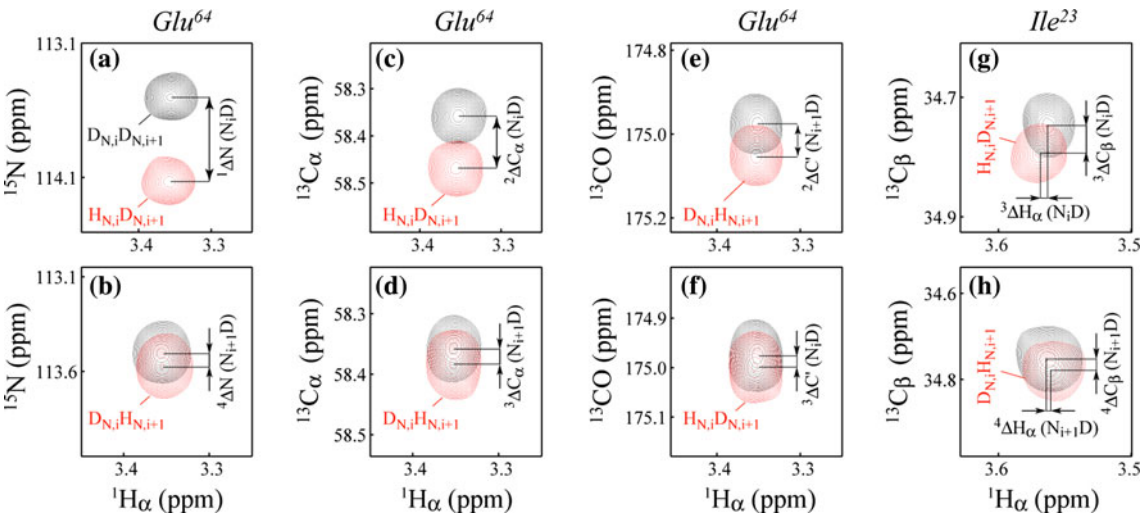

Fig. 3 Superposition of selected cross-peaks from 2D *intra*-HA[CA/CO/N/CB] correlation maps showing the displacement in peak positions arising from the $^1H \rightarrow D$ substitutions at backbone amide sites. Cross-peaks shown with *red*(*black*) contours correspond to the protonated(deuterated) molecular species as indicated on the plots using the notation defined in Fig. 2: **a**, **b** correlations of Glu^{64} of ubiquitin from the [$^1H_\alpha$–^{15}N] correlation map for measurements of **a** $^1\Delta N(N_iD)$ and **b** $^4\Delta N(N_{i+1}D)$ isotope shifts; **c**, **d** correlations of Glu^{64} from the [$^1H_\alpha$–$^{13}C_\alpha$] correlation map for measurements of **c** $^2\Delta C_\alpha(N_iD)$ and **d** $^3\Delta C_\alpha(N_{i+1}D)$ shifts; **e**, **f** correlations of Glu^{64} from the [$^1H_\alpha$–^{13}CO] correlation map for measurements of **e** $^2\Delta C'(N_{i+1}D)$ and **f** $^3\Delta C'(N_iD)$ shifts; **g**, **h** correlations of Ile^{23} of ubiquitin from the [$^1H_\alpha$–$^{13}C_\beta$] correlation map for measurements of **g** $^3\Delta C_\beta(N_iD)$ and **h** $^4\Delta C_\beta(N_{i+1}D)$ shifts. Displacements of peak positions in the acquisition ($^1H_\alpha$) dimension are indicated in **g** and **h** allowing the quantification of $^3\Delta H_\alpha(N_iD)$ and $^4\Delta H_\alpha(N_{i+1}D)$ isotope shifts

are small in magnitude, we have ascertained the consistency of the shifts derived from different combinations of sub-spectra. Figure S1 of the Supplementary Information shows the correlation plots of isotope shifts measured in GB1 illustrating the agreement between the shifts obtained from different pairs of datasets. The differences between the shifts quantified from different combinations of sub-spectra are small [pair-wise r.m.s.d of 3(7) ppb for $^{13}C_{\alpha}(^{15}N)$ shifts; Figure S1] and very similar in magnitude to the differences between the shifts obtained from duplicate measurements. However, since an excess of either solvent (H_2O or D_2O) in the sample solution (i.e. beyond 50 %) leads to the increase of probability to observe the fully protonated ($H_{N,i}H_{N,i+1}$) or fully deuterated ($D_{N,i}D_{N,i+1}$) species as a square of the fraction of this solvent [neglecting the differences arising from protium/deuterium fractionation ratios different from 1 (LiWang and Bax 1996)], significant differences in sensitivities of the sub-spectra selecting for different isotopic species of Fig. 2 may arise. For example, the sub-spectra selecting for the $H_{N,i}H_{N,i+1}$ species in ubiquitin were found to be on average 2.7 times less sensitive than the sub-spectra of the $D_{N,i}D_{N,i+1}$ species indicating that the deuterated amides were present at a $\sim$12 % excess (as in a 62 % D_2O/38 % H_2O solution if protium/deuterium fractionation is neglected). Therefore, we considered it more advantageous to measure all the isotope shifts in ubiquitin via the use of the most deuterated ($D_{N,i}D_{N,i+1}$) isotopic species (as it is shown in Fig. 3).

Below we describe each of the isotope effects arising from the $^1H_N \rightarrow D_N$ replacements at amide nitrogen positions (deuterium isotope shifts of ^{15}N, $^{13}C_{\alpha}$, ^{13}CO, $^{13}C_{\beta}$ and $^1H_{\alpha}$ nuclei) measured in the proteins ubiquitin and GB1 and, when possible, derive their dependence on protein local backbone geometry.

One- and four-bond ^{15}N isotope shifts: $^1\Delta N(N_iD)$ and $^4\Delta N(N_{i+1}D)$

The substitution of a directly attached proton nucleus for a deuteron at backbone amide positions results in by far the largest effect among those considered here—one-bond isotope effect on the chemical shift of nitrogen, $^1\Delta N(N_iD)$ (measured from the corresponding peak displacements in [$^1H_{\alpha}$–^{15}N] correlation maps; Fig. 3a). The average $^1\Delta N(N_iD)$ shift measured in both proteins is 687 ± 35 ppb ranging from 602(615) ppb for $Thr^9(Asp^{22})$ to 746(751) ppb for $Thr^{14}(Trp^{43})$ in ubiquitin(GB1). Full sets of $^1\Delta N(N_iD)$ values are shown versus residue numbers of each protein in Figure S2a, b of the Supplementary Information. The set of $^1\Delta N(N_iD)$ shifts measured in non-glycine residues of ubiquitin in the present work is in quantitative agreement with the values reported recently (Abildgaard et al. 2009) (pair-wise r.m.s.d between the two sets of data of 8.2 ppb) as illustrated in the correlation plot in Figure S2c (Supplementary Information).

$^1\Delta N(N_iD)$ shifts are weakly dependent on secondary structure (ϕ and ψ torsion angles) and are significantly affected by (1) geometries of hydrogen bonding at amide sites, and (2) the charges on neighboring (especially intra-residual) groups (Abildgaard et al. 2009). Following the analysis of (Abildgaard et al. 2009) and considering only aliphatic, non-polar residues in both ubiquitin and GB1 (glycines excluded) provides the following relationship for $^1\Delta N(N_iD)$ as a function of backbone dihedral angles and the hydrogen bond angle:

$$\begin{aligned} {}^1\Delta N(N_iD)(\text{ppb}) = {} & 689 + 13\sin(\phi + 117^\circ) \\ & + 43\cos(\psi - 60^\circ) \\ & + 16\cos(\Theta_{N-H\cdots O}) \end{aligned} \quad (3)$$

where $\Theta_{N-H\cdots O}$ is the angle formed between N–H and the direction of a hydrogen bond in the crystal structures of ubiquitin and GB1 (180° for the linear bond; assumed equal to 90° for non-hydrogen-bonded amides). This result is to be compared with $^1\Delta N(N_iD)$ (ppb) = 660 + 60-sin (ϕ + 88°) + 43cos (ψ − 68°) + 30cos ($\Theta_{N-H\cdots O}$), obtained by (Abildgaard et al. 2009) for ubiquitin only (including glycines) using ab initio-optimized geometries of hydrogen bonds. The correlation plot comparing experimental $^1\Delta N(N_iD)$ isotope shifts measured in ubiquitin and GB1 for 29 non-glycine residues with aliphatic, non-polar side-chains and the values calculated using Eq. 3 is shown in Figure S2d (Supplementary Information). Although the overall agreement between the two sets of shifts (pair-wise r.m.s.d = 14.9 ppb) is close to that obtained for ubiquitin (14 ppb) (Abildgaard et al. 2009), we note that the largest discrepancies are obtained for Ile^{61} in ubiquitin and Val^{54} and Phe^{30} in GB1 (color-coded in Figure S2d). Interestingly, the amide of Ile^{61} is involved in one of the weakest hydrogen bonds in ubiquitin ($r_{N-H\cdots O} > 2.4$ Å), and its effect may not be adequately described by the last term in Eq. 3, while the side-chain of Val^{54} in GB1 adopts a very rare for valines *gauche*(−) conformation placing both methyl groups in the vicinity of the amide moiety.

The most intriguing are four-bond isotope effects on ^{15}N chemical shifts resulting from ^1H-to-D substitution at the amides of the following (i + 1) residues, $^4\Delta N(N_{i+1}D)$ (see Fig. 3b illustrating the corresponding displacement of peak positions in [$^1H_{\alpha}$–^{15}N] spectra). These higher order effects on ^{15}N chemical shifts are surprisingly large and uniformly positive: the average value of 34 ± 12 ppb is calculated for the combined set values in ubiquitin and GB1 ranging from 13 ppb for $Lys^{33}(Glu^{19})$ in ubiquitin (GB1) to 68 ppb for Glu^{64} in ubiquitin. Although the $^4\Delta N(N_{i+1}D)$ effects do

not show clear dependence on the secondary structure in the sense that it may be too complex for a satisfactory description by simple trigonometric relationships, we noted that $^4\Delta N(N_{i+1}D)$ shifts show some dependence on the distance between nitrogen and the amide $^1H/D$ of the following residue where the ^1H–D substitution occurs, $r_{N-NH,i+1}$. Figure 4 shows the $^4\Delta N(N_{i+1}D)$ shifts in ubiquitin (black circles) and GB1 (red circles) plotted versus the distance $r_{N-NH,i+1}$. Notably, the set of largest values of $^4\Delta N(N_{i+1}D)$ shifts corresponds to the shortest $r_{N-NH,i+1}$ distances in both proteins. In β-structures (including the regions of extended coil), $r_{N-NH,i+1}$ adopt a wide range of values between ~3.4 and 4.1 Å, while in regular α-helices much shorter distances are measured—usually, falling in the range between 2.4 and 2.6 Å (Fig. 4). The most pronounced $^4\Delta N(N_{i+1}D)$ effects (larger shifts) in both proteins correspond to exceptionally short $r_{N-NH,i+1}$ values (<2.4 Å), which are commonly observed in the bends of the polypeptide chain, short 3_{10}-helical stretches or C-terminal residues of α-helices. Almost all the residues with $^4\Delta N(N_{i+1}D)$ shifts higher than ~45 ppb in both proteins (Fig. 4) belong to these regions of secondary structure. Ile^{13} of ubiquitin has unusually high $^4\Delta N(N_{i+1}D)$ value despite that it is located in a β-sheet (Fig. 4). Interestingly, the amide of Ile^{13} forms one of the strongest hydrogen bond in the protein with the carbonyl oxygen of Val^5 ($r_{N-H\cdots O} = 1.7$ Å).

A more quantitative description of $^4\Delta N(N_{i+1}D)$ as a function of $r_{N-NH,i+1}$ (such as, for example, fitting of the $^4\Delta N(N_{i+1}D)$ values to a Morse-type potential functional

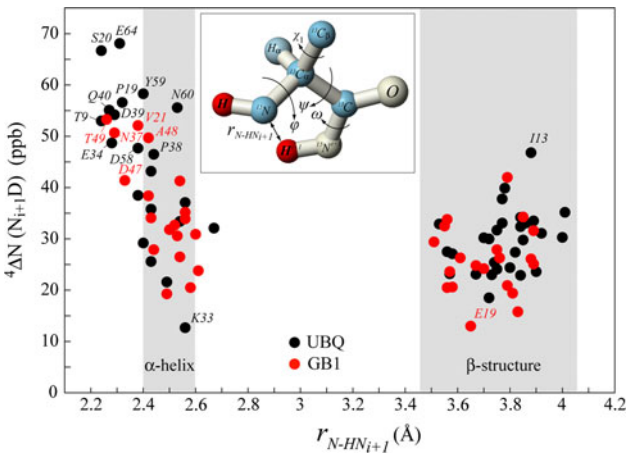

Fig. 4 A plot showing the measured four-bond $^4\Delta N(N_{i+1}D)$ shifts (ppb) in ubiquitin (*black circles*) and GB1 (*red circles*) versus the distance between amide nitrogen and the amide $^1H/D$ of the following residue, $r_{N-NH,i+1}$ (Å). The regions of $r_{N-NH,i+1}$ distances corresponding to regular α-helices and β-structures (including extended coil regions) are shaded. The *inset* shows a fragment of a polypeptide chain with the distance $r_{N-NH,i+1}$ indicated by an *arrow*. The residues with outstanding values of $^4\Delta N(N_{i+1}D)$ shifts in each protein are labeled with residue types and numbers

form) does not provide satisfactory results—in part, due a large scatter of experimental $^4\Delta N(N_{i+1}D)$ values corresponding to higher $r_{N-NH,i+1}$ distances (β-regions, coil; Fig. 4). Nevertheless, we note that the observed correlation of $^4\Delta N(N_{i+1}D)$ shifts with $r_{N-NH,i+1}$ in the region of short $r_{N-NH,i+1}$ distances is qualitatively consistent with earlier observations that ^{13}C four-bond deuterium isotope shifts in small organic molecules result primarily from 'through-space' interactions of the nucleus whose isotope shift is observed with the dipole where the ^1H-to-D replacement occurs (Anet and Dekmezian 1979; Aydin and Günther 1981; Ernst et al. 1982; Majerski et al. 1985) (i.e. ^{15}N with the $^{15}N_{i+1}$–$^1H/D_{i+1}$ dipole in the present case). Of note, the four-bond ^{15}N isotope effects arising from the $^1H \rightarrow D$ substitution at the amides of preceding residues ($i - 1$) are not resolved in our measurements and are expected to contribute equally to the line-widths of all cross-peaks in the [$^1H_\alpha$–^{15}N] correlation maps.

Three- and two-bond $^{13}C_\alpha$ isotope shifts: $^3\Delta C_\alpha(N_{i+1}D)$ and $^2\Delta C_\alpha(N_iD)$

Three-bond $^{13}C_\alpha$ isotope shifts resulting from $^1H \rightarrow D$ substitutions at N_{i+1} positions, $^3\Delta C_\alpha(N_{i+1}D)$, and two-bond $^{13}C_\alpha$ shifts resulting from $^1H \rightarrow D$ substitutions at positions N_i, $^2\Delta C_\alpha(N_iD)$, have been measured from the corresponding peak displacements in [$^1H_\alpha$–$^{13}C_\alpha$] correlation maps shown in Fig. 3c, d. In ubiquitin, the values of $^3\Delta C_\alpha(N_{i+1}D)$ and $^2\Delta C_\alpha(N_iD)$ shifts measured using the scheme of Fig. 1 are in good agreement with the set of values reported earlier from 3D HACAN and HACA(CO)N experiments by (Ottiger and Bax 1997) (pair-wise r.m.s.d of 2.9 and 3.4 ppb for the $^3\Delta C_\alpha(N_{i+1}D)$ and $^2\Delta C_\alpha(N_iD)$ shifts, respectively; see Figure S3 of the Supplementary Information showing the correlation plot comparing the two sets of data).

The $^3\Delta C_\alpha(N_{i+1}D)$ shifts vary from 8(12) ppb for Asp^{52}(Phe^{30}) to 52(50) ppb for Ile^{61}(Ile^6) in ubiquitin(GB1) (the average shift is 31 ± 13 ppb). An interesting relationship that describes the dependence of $^3\Delta C_\alpha(N_{i+1}D)$ on ψ torsion angles, has been noted by (Ottiger and Bax 1997): $A + B\sin(\psi + C)$. Note that ψ is not the dihedral angle formed by the intervening bonds in the case of $^3\Delta C_\alpha(N_{i+1}D)$ shifts, as this role is taken up by the (fixed) angle of the peptide bond, ω. Upon exclusion of all the residues preceding glycines, non-glycine residues with positive ϕ angles and residues disordered in solution (Leu^8–Lys^{11}, Arg^{72}–Arg^{74} in ubiquitin and Lys^{10}, Thr^{11} and Asn^{37}–Asp^{40} in GB1), the least squares fit of the combined set of ubiquitin and GB1 $^3\Delta C_\alpha(N_{i+1}D)$ shifts yields:

$$^3\Delta C_\alpha(N_{i+1}D)(\text{ppb}) = 29 + 17\sin(\psi - 13^\circ) \quad (4)$$

with the r.m.s.d. between the measured and back-calculated shifts of 3.6 ppb (Fig. 5a)—more than an order of

magnitude lower than the range of $^{3}\Delta N(C_{\alpha,i-1}D)$ values ($\sim$40 ppb). This result compares well with the parameterization of $^{3}\Delta C_{\alpha}(N_{i+1}D)$ of (Ottiger and Bax 1997) on ubiquitin data: $^{3}\Delta C_{\alpha}(N_{i+1}D)$ (ppb) = 30 + 22sin (ψ − 4°) with the pair-wise r.m.s.d. = 3.4 ppb between the experimental and back-calculated values. The residues that precede glycines in the amino-acid sequence of ubiquitin and GB1 and the residues with positive ϕ angles (color-coded in Fig. 5a) have the $^{3}\Delta C_{\alpha}(N_{i+1}D)$ values significantly lower than predicted by Eq. 4 and have been excluded from the fit.

The $^{2}\Delta C_{\alpha}(N_{i}D)$ isotope shifts vary from 75(76) ppb for Thr^{7}(Tyr^{3}) to 116(107) ppb for Ala^{46}(Lys^{50}) in ubiquitin(GB1) with the average value of 91 ± 8 ppb (C-terminal residues of GB1 excluded). Non-glycine residues having positive ϕ angles in both proteins (Ala^{46}, Asn^{60}, Glu^{64} in ubiquitin; Lys^{50} in GB1) showing the largest isotope effects. The fit of the combined set of $^{2}\Delta C_{\alpha}(N_{i}D)$ shifts in ubiquitin and GB1 yields:

$$^{2}\Delta C_{\alpha}(N_{i}D)(\text{ppb}) = 96 + 8\sin(\phi + 39^{\circ}) + 9\sin(\psi + 47^{\circ}) \quad (5)$$

with the r.m.s.d between experimental and back-calculated values of 4.6 ppb. This result compares well with the parameterization of (Ottiger and Bax 1997) on ubiquitin: $^{2}\Delta C_{\alpha}(N_{i}D)$ (ppb) = 93 + 10sin (ϕ + 62°) + 12sin (ψ + 42°) with the r.m.s.d of 4.1 ppb between experimental and back-calculated values. Figure 5b shows the comparison of experimental $^{2}\Delta C_{\alpha}(N_{i}D)$ shifts of ubiquitin and GB1 with the shifts calculated using Eq. 5. A number of residues with outstanding disagreements between the measured and calculated values can be noted: Lys^{11}, Asp^{21}, Glu^{24} and Phe^{45} in ubiquitin and Leu^{12}, Ala^{20}, Ala^{48}, Thr^{49} in GB1. Of note, the $^{2}\Delta C_{\alpha}(N_{i}D)$ values of Lys^{11}, Asp^{21} and Glu^{24} of ubiquitin could not be measured with confidence in the study of (Ottiger and Bax 1997) and were excluded from the fit. However, their values have been confirmed to within random errors in this work and therefore included in analysis. Phe^{45} has also been reported as a clear 'outlier' in the study of (Ottiger and Bax 1997) but included in the fit. The reasons for (usually) higher than predicted $^{2}\Delta C_{\alpha}(N_{i}D)$ values for these residues in both proteins (color-coded in Fig. 5b) remain unclear. Their exclusion from the fit provides essentially the same set of parameters as in Eq. 5, but reduces the r.m.s.d between experimental and back-calculated values to 4.0 ppb.

Three- and two-bond isotope effects on carbonyl carbon chemical shifts: $^{3}\Delta C'(N_{i}D)$ and $^{2}\Delta C'(N_{i+1}D)$

Three-bond(two-bond) ^{13}CO isotope shifts resulting from the ^{1}H → D substitutions at $N_{i}(N_{i+1})$ positions, $^{3}\Delta C'(N_{i}D)$ ($^{2}\Delta C'(N_{i+1}D)$), are measured from the displacements in peak positions of [H_{α}–^{13}CO] correlation maps as shown in Fig. 3e, f).

The $^{3}\Delta C'(N_{i}D)$ isotope shifts are positive and vary from 1(2) ppb for Ser^{20}(Lys^{28}) to 35(36) ppb for Val^{70}(Ala^{20}) in ubiquitin(GB1) covering approximately the same range of values as the $^{3}\Delta C'(C_{\alpha,i+1}D)$ shifts arising from ^{1}H → D substitutions at $^{13}C_{\alpha}$ sites of the following residue reported by us recently (Sun and Tugarinov 2012). The average value of $^{3}\Delta C'(N_{i}D)$ in the combined set of shifts in both proteins is 17 ± 7 ppb. The $^{3}\Delta C'(N_{i}D)$ isotope shifts

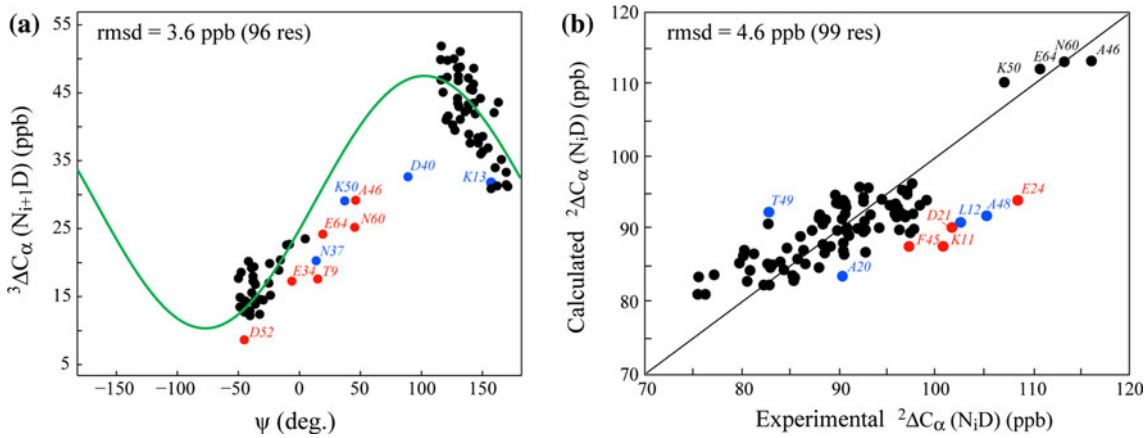

Fig. 5 **a** Three-bond $^{3}\Delta C_{\alpha}(N_{i+1}D)$ isotope shifts (ppb) measured in ubiquitin and GB1 plotted as a function of dihedral angle ψ (deg.) derived from the crystallographic structures with PDB id codes 1ubq (Vijay-Kumar et al. 1987) and 2qmt (Frericks-Schmidt et al. 2007). The green curve corresponds to the relationship in Eq. 4. Residues preceding glycines and the non-glycine residues with *positive* ϕ angles (Ala^{46}, Asn^{60}, Glu^{64} in ubiquitin; Lys^{50} in GB1) are shown in *red* (ubiquitin) and *blue (GB1)* and labeled with residue numbers. In both proteins, these residues show higher than predicted values of $^{3}\Delta C_{\alpha}(N_{i+1}D)$ and were excluded from analysis. **b** A correlation plot comparing experimental two-bond $^{2}\Delta C_{\alpha}(N_{i}D)$ isotope shifts (ppb) of ubiquitin and GB1 (*x*-axis) with the shifts calculated using Eq. 5 (*y*-axis). Residues shown in *red* (ubiquitin) and *blue* (GB1) show the largest disagreements with the values predicted by Eq. 5

measured in ubiquitin(GB1) are plotted versus residue numbers of the two proteins in Fig. 6a, b). Although some dependence of $^{3}\Delta C'(N_iD)$ on the secondary structure is apparent (mostly due to the variation of the angle ϕ which is in this case the dihedral angle formed by the three intervening bonds), with somewhat lower values associated with α-helices in both proteins (Glu^{24} in ubiquitin is a reproducible exception; Fig. 6a), the best-fit of $^{3}\Delta C'(N_iD)$ to trigonometric functional form involving ϕ and/or ψ angles results in a large scatter between the measured and back-calculated values. A very limited set of 7 $^{3}\Delta C'(N_iD)$ shifts ranging from 26 to 50 ppb has been measured earlier in BPTI by Tüchsen and Hansen (Tüchsen and Hansen 1991). The authors related the $^{3}\Delta C'(N_iD)$ values to the distances between carbonyl oxygens and the amide $^{1}H/D$ sites of the same residue, $r_{O–HN}$, with the largest $^{3}\Delta C'(N_iD)$ values in BPTI corresponding to the shortest $r_{O–HN}$ distances (encountered in extended structures: coils and β-sheets). The plot of all $^{3}\Delta C'(N_iD)$ shifts measured in ubiquitin and GB1 versus $r_{O–HN}$ is provided in Figure S4 of the Supplementary Information. The use of a much larger subset of $^{3}\Delta C'(N_iD)$ values in this study (112) shows that the dependence of $^{3}\Delta C'(N_iD)$ on the $r_{O–HN}$ distances is mostly notable for $r_{O–HN} < 3.5$ Å (i.e. for the regions with extended polypeptide backbone conformations). A significant degree of overlap between the $^{3}\Delta C'(N_iD)$ shifts corresponding to low and high $r_{O–HN}$ distances (Figure S4) implies that $^{3}\Delta C'(N_iD)$ effects are not exclusively of electrostatic nature.

Two-bond $^{2}\Delta C'(N_{i+1}D)$ isotope shifts were measured earlier in BPTI by Tüchsen and Hansen (1991) and utilized to quantify protium/deuterium fractionation at amide positions of ubiquitin (LiWang and Bax 1996). The average $^{2}\Delta C'(N_{i+1}D)$ value of 84 ± 5(77 ± 7) ppb has been obtained then in ubiquitin(BPTI). A combined histogram plot of two-bond $^{2}\Delta C'(N_{i+1}D)$ isotope shifts measured in ubiquitin and GB1 is shown in Fig. 6c. The average value of 82 ± 6 ppb has been calculated for the combined set of shifts from the two proteins. By absolute magnitude, the $^{2}\Delta C'(N_{i+1}D)$ effects are ~eightfold larger than the $^{2}\Delta C'(C_{\alpha,i}D)$ shifts arising from $^{1}H \rightarrow D$ substitutions at $^{13}C_\alpha$ sites of the same residue (Sun and Tugarinov 2012). In agreement with earlier observations (Tüchsen and Hansen 1991), the variability of $^{2}\Delta C'(N_{i+1}D)$ shifts is quite low, with most of the residues having values between 75 and 90 ppb (Fig. 6c). The small range of variation precludes their interpretation in terms of backbone geometry. However, no dependence of $^{2}\Delta C'(N_{i+1}D)$ shifts on ϕ or ψ angles can be expected as carbonyl carbon nuclei are separated from the site of deuteration by a non-free-rotatable peptide bond. Tüchsen and Hansen have used the $^{2}\Delta C'(N_{i+1}D)$ shifts for rough estimation of hydrogen bonding enthalpies in BPTI (Tüchsen and Hansen 1991).

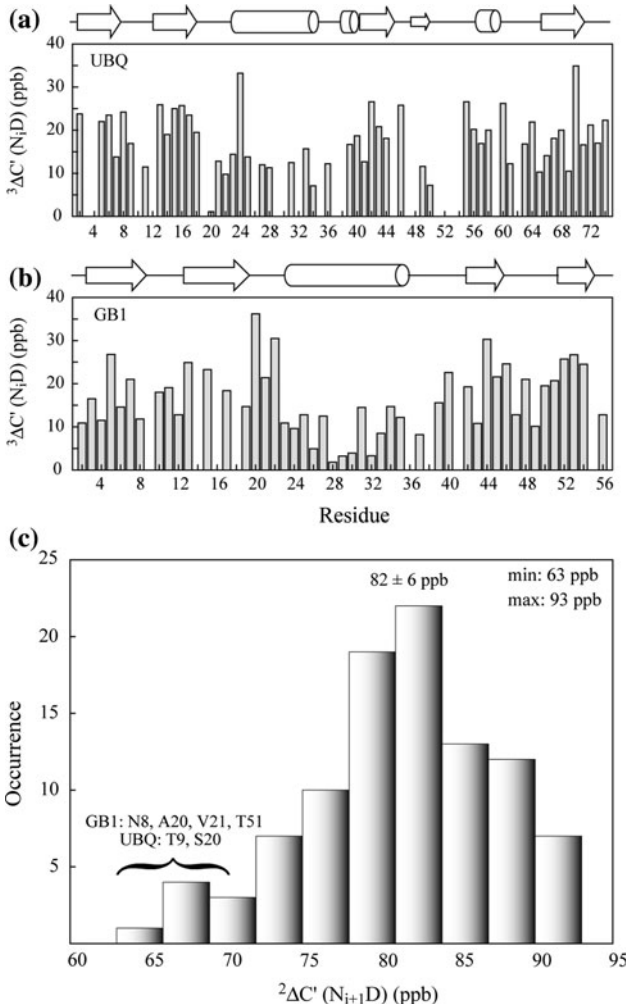

Fig. 6 Three-bond $^{3}\Delta C'(N_iD)$ isotope shifts (ppb) measured in **a** ubiquitin and **b** GB1 plotted versus residue numbers of the two proteins. **c** A combined histogram plot of two-bond $^{2}\Delta C'(N_{i+1}D)$ isotope shifts (ppb) measured in ubiquitin and GB1. The mean value ±1 standard deviation of the distribution as well as the maximal and minimal observed shifts are indicated on the plot. The residues with the lowest $^{2}\Delta C'(N_{i+1}D)$ values (<70 ppb) in each protein are listed. Schematic diagrams of the secondary structures of ubiquitin and GB1 are shown above panels **a**, **b** with *arrows* and *cylinders* denoting β-strands and *helices*, respectively

Notably, in several residues of ubiquitin and GB1 the $^{2}\Delta C'(N_{i+1}D)$ values are lower than 70 ppb (listed in Fig. 6c). Four of these sites (Thr^{9}, Ser^{20} in ubiquitin, and Ala^{20}, Val^{21} in GB1) are located in the loops or at the very start of secondary structure elements, and their carbonyls do not participate in hydrogen bonds.

One- and four-bond deuterium isotope effects on $^{13}C_\beta$ chemical shifts: $^{3}\Delta C_\beta(N_iD)$ and $^{4}\Delta C_\beta(N_{i+1}D)$

Three-bond(four-bond) $^{13}C_\beta$ isotope shifts resulting from $^{1}H \rightarrow D$ substitutions at $N_i(N_{i+1})$ positions, $^{3}\Delta C_\beta(N_iD)$($^{4}\Delta C_\beta(N_{i+1}D)$, have been measured from the corresponding peak

displacements in [$^{1}H_{\alpha}$–$^{13}C_{\beta}$] correlation maps as shown in Fig. 3g, h). Since the $^{1}H_{\alpha}$–$^{13}C_{\beta}$ correlations in these 2D maps (acquired with the inset '$^{13}C_{\beta}$' of the pulse-scheme in Fig. 1) are of quite low sensitivity even after prolonged acquisitions (see "Materials and methods") we have performed additional measurements of $^{3}\Delta C_{\beta}(N_iD)$ and $^{4}\Delta C_{\beta}(N_{i+1}D)$ shifts using more sensitive 3D HACBN(H/D) experiments ingeniously crafted earlier by (Meissner and Sørensen 1998) specifically for the measurement of these $^{13}C_{\beta}$ isotope effects. These experiments correlate the chemical shifts of $^{1}H_{\alpha}$ nuclei with $^{13}C_{\beta}$ of the same residue and ^{15}N nuclei of residues i and $i + 1$ (N_i and N_{i+1}) with the BIRD $^{1}H/D$ filtering on both nitrogens, and thus allow measuring the $^{3}\Delta C_{\beta}(N_iD)$ and $^{4}\Delta C_{\beta}(N_{i+1}D)$ shifts from the intra- and inter-residual cross-peaks, respectively. The values of $^{3}\Delta C_{\beta}(N_iD)$ and $^{4}\Delta C_{\beta}(N_{i+1}D)$ reported here represent the subsets of those isotope shifts in ubiquitin and GB1 that are reproducible between the 2D [$^{1}H_{\alpha}$–$^{13}C_{\beta}$] correlation maps and the 3D HACBN(H/D) spectra or could be measured with confidence in either dataset.

Figure 7 shows the $^{3}\Delta C_{\beta}(N_iD)$ isotope shifts plotted versus residue numbers of ubiquitin and GB1 (Fig. 7a, c) aligned along the plots of dihedral angles ϕ (grey shaded bars) and χ_1 (open red bars) of each protein (Fig. 7b, d). The range of values covered by $^{3}\Delta C_{\beta}(N_iD)$ shifts is somewhat larger than that of $^{3}\Delta C_{\alpha}(N_{i+1}D)$ shifts: from 7(2) ppb for Ala^{46}(Ala^{20}) to 61(65) ppb for Gln^{31}(Tyr^{33}) in ubiquitin(GB1) (average $^{3}\Delta C_{\alpha}(N_{i+1}D)$ in both proteins is 37 ± 16 ppb). It is immediately clear from Fig. 7a, c that uniformly higher $^{3}\Delta C_{\beta}(N_iD)$ shifts are observed in the helical regions and some turns of both proteins (corresponding to lower absolute values of ϕ angles). The interpretation of $^{3}\Delta C_{\beta}(N_iD)$ in terms of dihedral angles is, however, more complex than for $^{3}\Delta C_{\alpha}(N_{i+1}D)$ shifts and is compounded by a number of factors: (1) the effects of substituents on β-carbons (hydroxyl groups in Ser, Thr; aromatic rings in Phe, Tyr and Trp), β-branching in Val, Ile side-chains and/or (2) an additional dependence of $^{3}\Delta C_{\beta}(N_iD)$ on side-chain χ_1 dihedral angles that may undergo rotamer averaging. Remarkably, the $^{3}\Delta C_{\beta}(N_iD)$ shifts of Thr and β-branched residues (Val and Ile) that adopt *gauche*(−) conformations around the χ_1 angle ($\chi_1 \approx +60°$) have very small $^{3}\Delta C_{\beta}(N_iD)$ shifts: Ile^{3}, Thr^{7}, Thr^{9}, Thr^{22}, Thr^{55} in ubiquitin (Fig. 7a, b) and Thr^{17}, Thr^{44}, Thr^{49}, Thr^{53}, Val^{54} in GB1 (Fig. 7c, d) all have shifts below 13 ppb. Thr^{14} in ubiquitin with the relatively high $^{3}\Delta C_{\beta}(N_iD)$ value of 26 ppb is apparently an exception, but its χ_1 angle is not reproducible in other structures of the protein. In GB1, also Thr^{11} with negative χ_1 and Ala^{20} have $^{3}\Delta C_{\beta}(N_iD)$ values below 5 ppb—however, both residues are located in loops and may have certain flexibility around the ϕ and/or χ_1 angles (note also the low $^{2}\Delta C'(N_{i+1}D)$ value in Ala^{20} of GB1; Fig. 6c). Anomalously low values of isotope shifts may also result from fast exchange of amide protons/deuterons with the solvent at these residues at a relatively high pH (6.0) of the GB1 sample. Threonine residues dominate the list of residues with very low $^{3}\Delta C_{\beta}(N_iD)$ values because (as with Ile side-chains) in threonines the *gauche*(−) conformation around χ_1 is almost as probable as *gauche*(+) (Dunbrack 2002; Kehl et al. 2008; Lovell et al. 2000; Scouras and Daggett 2011; Van der Kamp et al. 2010). Interestingly, non-glycine residues with positive ϕ angles (Ala^{46}, Asn^{60}, Glu^{64} in ubiquitin and Lys^{50} in GB1; Fig. 7) are also characterized by very low $^{3}\Delta C_{\beta}(N_iD)$ shifts.

Initial attempts to interpret $^{3}\Delta C_{\beta}(N_iD)$ via Karplus-type relationships that include angle ϕ (the angle formed by the three intervening bonds) and the side-chain angle χ_1 have shown that statistically significant increase in the

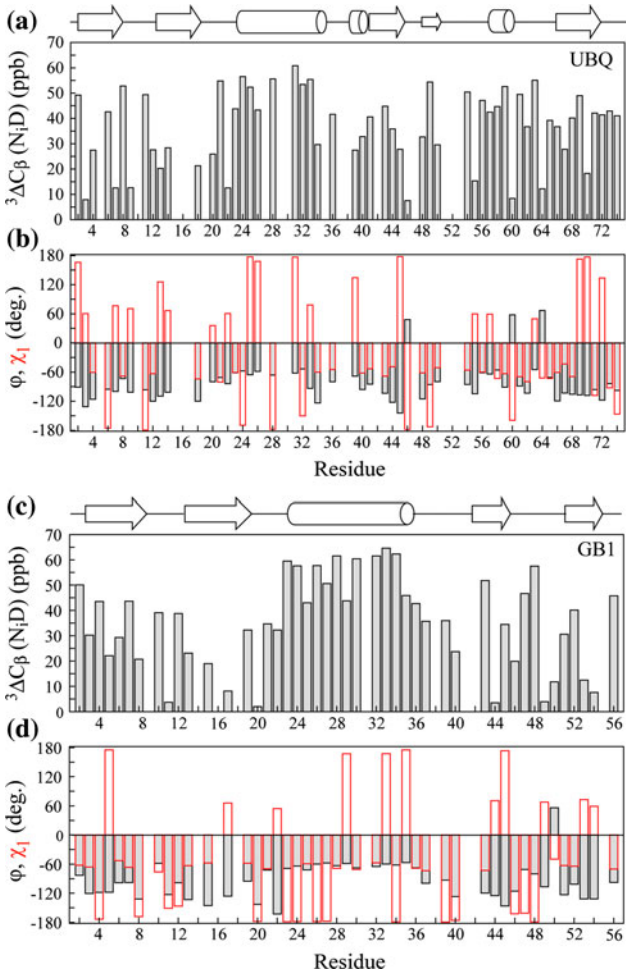

Fig. 7 Three-bond $^{3}\Delta C_{\beta}(N_iD)$ isotope shifts (ppb) plotted versus residue numbers for **a** ubiquitin and **c** GB1. Panels **b** and **d** the plots of dihedral angles ϕ (*grey shaded bars*) and χ_1 (*open red bars*) (both in degrees) for the two proteins derived from the crystallographic structures with PDB id codes 1ubq and 2qmt. Schematic diagrams of the secondary structure of ubiquitin and GB1 are shown above panels **a** and **c**, with *arrows* and *cylinders* denoting β-strands and *helices*, respectively

agreement between experimental and back-calculated values is achieved if only residues with χ_1 corresponding to the most probable orientations of the side-chains around the C_α–C_β bond (i.e. *gauche*(+) with $\chi_1 \approx -60°$ and trans with $\chi_1 \approx 180°$) are included in analysis. Therefore, we have excluded all residues with much less probable *gauche*(−) and eclipsed (χ_1 close to 0° or ±120°) side-chain conformations (associated with very low $^3\Delta C_\beta(N_iD)$ in Thr, Val and Ile) as well as alanines. The best description of $^3\Delta C_\beta(N_iD)$ shifts provided by the least-squares fit of ϕ and χ_1 angles of all non-alanine residues in ubiquitin and GB1 with either *gauche*(+) or trans side-chain conformations (Thr[11] in GB1 was also excluded) is given by

$$^3\Delta C_\beta(N_iD)(\text{ppb}) = 17 - 30\sin(\phi - 42°) - 7\sin(\chi_1 + 36°) \quad (6)$$

with the pair-wise r.m.s.d between experimental and back-calculated values of 7.2 ppb for 66 residues. Contrary to theoretical predictions showing that $^3\Delta C_\beta(N_iD)$ should depend on *both* ϕ and ψ angles (Hansen 2000), no statistically significant improvement in the fit was observed upon inclusion of ψ-dependent terms into Eq. 6. Figure 8a shows the subset of three-bond $^3\Delta C_\beta(N_iD)$ isotope shifts of non-Ala residues with either *gauche*(+) or trans conformations around χ_1 angles measured in both proteins, plotted as a function of dihedral angles ϕ. The correlation plot comparing experimental $^3\Delta C_\beta(N_iD)$ shifts for the analyzed subset of residues in ubiquitin and GB1 with the shifts calculated using Eq. 6, is shown in Fig. 8b. A number of residues in both proteins show large disagreements between experimental and back-calculated values (color-coded in Fig. 8a, b). It can be noted that aromatic residues comprise a high proportion (5 out of 9) of these sites (Phe[45] and Tyr[59] in ubiquitin and Phe[30], Tyr[33], Tyr[45] in GB1). Exclusion of these aromatic residues together with all the other sites color-coded in Fig. 8, changes the r.m.s.d of the fit to 5.9 ppb for 57 residues without significantly affecting the parameters of Eq. 6. Of note, because of the sp2-hydridization of γ carbons in Phe and Tyr, χ_2 angles of these residues very rarely adopt a trans ($\chi_2 \approx 180°$) configuration as this would lead to an eclipsed state around χ_2 (Dunbrack 2002; Kehl et al. 2008; Lovell et al. 2000; Scouras and Daggett 2011; Van der Kamp et al. 2010).

It is important to realize that the analysis of $^3\Delta C_\beta(N_iD)$ effects in terms of backbone and side-chain geometry described above is only semi-quantitative as it disregards the fact that many side-chains may undergo rotamer averaging in solution fast on the chemical shift time-scale, and thus necessarily 'over-relies' upon crystallographic data. Statistically, however, the inclusion of the last term in Eq. 6 leads to an improvement of the fit by 2.0(1.8) ppb when the residues with *gauche*(−) and eclipsed conformations around χ_1 and alanines are excluded even though some of the χ_1 angles in solution may differ from those in the 1.8(1.0)Å crystal structures of ubiquitin(GB1)—especially in the residues located in loops and coils, i.e. not involved in secondary structure elements.

The four bond effects on $^{13}C_\beta$ nuclei, $^4\Delta C_\beta(N_{i+1}D)$, could be measured only with low accuracy for about ½ of the residues in each protein. Figure S5 (Supplementary Information) shows a combined histogram plot of the four-bond $^4\Delta C_\beta(N_{i+1}D)$ isotope shifts that could be measured with confidence in ubiquitin and GB1 and which were found reproducible to within two standard deviations between the 2D [$^1H_\alpha$–$^{13}C_\beta$] correlation maps and the

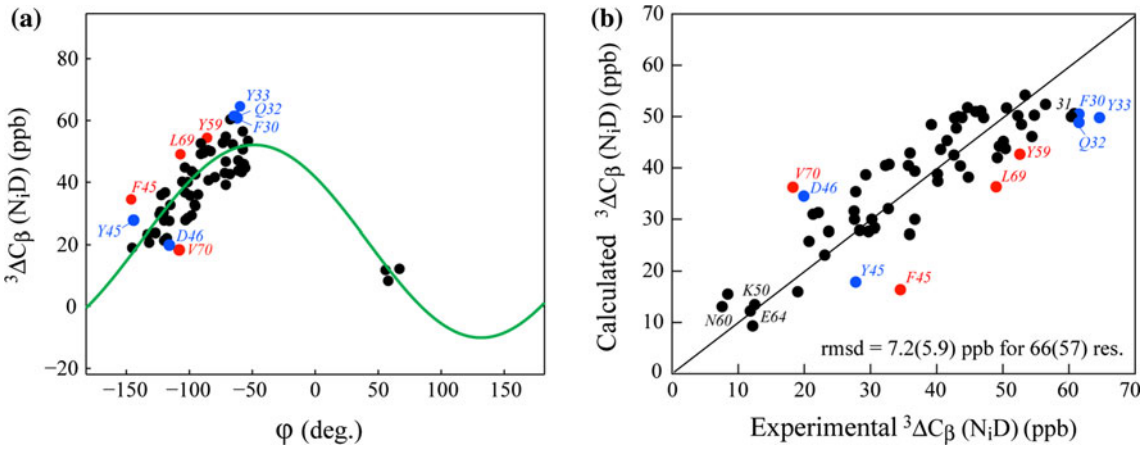

Fig. 8 **a** A subset of three-bond $^3\Delta C_\beta(N_iD)$ isotope shifts (ppb) of non-Ala residues with either gauche(+) or trans conformations around χ_1 angles measured in ubiquitin and GB1 plotted as a function of dihedral angles ϕ (deg.). The *green curve* is drawn using the relationship in Eq. 6 with χ_1 fixed at −60° [*gauche*(+) conformation]. **b** A correlation plot of experimental $^3\Delta C\beta(N_iD)$ isotope shifts for the subset of ubiquitin and GB1 residues shown in **a** (*x*-axis) with the shifts calculated using Eq. 6 (*y*-axis). Residues shown in *red* (ubiquitin) and *blue* (GB1) show the largest disagreements with the values predicted by Eq. 6

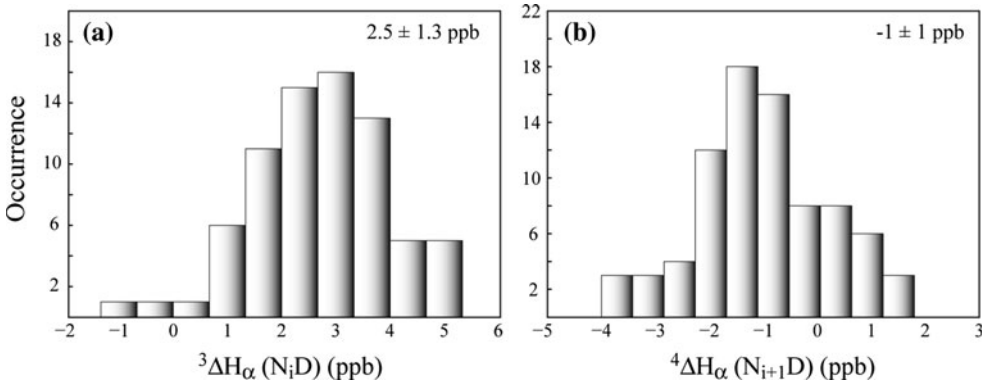

Fig. 9 Histogram plots of **a** three-bond $^3\Delta H_\alpha(N_iD)$, and **b** $^4\Delta H_\alpha(N_{i+1}D)$ isotope shifts (ppb) that could be measured with confidence in ubiquitin and GB1. Mean values ±1 standard deviation of each distribution are indicated in the *top right corners* of the plots

3D HACBN(H/D) spectra. The mean value of the $^4\Delta C_\beta(N_{i+1}D)$ distribution is positive (5 ppb), but a relatively large range of variability of these effects can be noted (from −10 ppb for several residues in both proteins up to 25–28 ppb for a pair of α-helical residues in GB1; Figure S5). Although the average value of $^4\Delta C_\beta(N_{i+1}D)$ is very similar to that observed by us for the four-bond $^{13}C_\alpha$ effects arising from the ^{1}H-to-D replacement at α-carbon of a previous residue, $^4\Delta C_\alpha(C_{\alpha,i-1}D)$ (Sun and Tugarinov 2012), the range of $^4\Delta C_\beta(N_{i+1}D)$ variability is approximately threefold larger.

Three- and four-bond α-proton isotope shifts, $^3\Delta H_\alpha(N_iD)$ and $^4\Delta H_\alpha(N_{i+1}D)$

Three-bond(four-bond) $^1H_\alpha$ isotope shifts resulting from $^1H \rightarrow D$ substitutions at $N_i(N_{i+1})$ can be estimated from any of the four types of correlation maps included in Fig. 3. These shifts are shown in Fig. 3g, h) as peak displacements in the acquisition ($^1H_\alpha$) dimension of the [$^1H_\alpha$–$^{13}C_\beta$] correlation maps. However, the two most sensitive correlation maps, [$^1H_\alpha$–$^{13}C_\alpha$] and [$^1H_\alpha$–^{13}CO], are better candidates for the measurements of these very small effects. Figure S6 of the Supplementary Information shows the correlation plot comparing $^3\Delta H_\alpha(N_iD)$ isotope effects measured in ubiquitin and GB1 from the [$^1H_\alpha$–$^{13}C_\alpha$] and [$^1H_\alpha$–^{13}CO] spectra. Only the values that were found reproducible between these two measurements to within two pair-wise r.m.s.d's (2.5 ppb) are included in the combined histogram plot of $^3\Delta H_\alpha(N_iD)$ shifts in ubiquitin and GB1 in Fig. 9a. These three-bond effects are predominantly positive (the mean of 2.5 ± 1.3 ppb), but some reproducible excursions to small negative values are observed in both proteins. The range of these shifts (from −1 to 5 ppb) is almost twice smaller than the range of values we reported recently for their amide proton counterparts, $^3\Delta H_N(C_{\alpha,i}D)$ shifts arising from deuteration of $^{13}C_\alpha$ positions (~10 ppb) (Sun and Tugarinov 2012). The four-bond effects, $^4\Delta H_\alpha(N_{i+1}D)$, are, as expected, even smaller and cannot be measured accurately because their absolute magnitude is often lower than the error in the measurement of the displacement in peak positions. The combined histogram of $^4\Delta H_\alpha(N_{i+1}D)$ values for ubiquitin and GB1 is shown in Fig. 9b. Statistically, the values of $^4\Delta H_\alpha(N_{i+1}D)$ have higher probability to be negative (−1 ppb on average) but a number of positive values could be reproducibly observed in both proteins.

Concluding remarks

In summary, we described an approach for accurate measurements of deuterium isotope effects on the chemical shifts of ^{15}N, $^{13}C_\alpha$, $^{13}C_\beta$, ^{13}CO and $^1H_\alpha$ nuclei in proteins arising from ^{1}H-to-D substitutions at backbone amides. The comparison of chemical shifts in the spectra selecting for the molecular species with a defined isotopic content at successive backbone nitrogen positions shown in Fig. 2, provides the one- to four-bond deuterium isotope shifts of all the backbone and $^{13}C_\beta$ sites in a protein. Although all the shifts that have been quantified using the scheme of Fig. 1 are described here, the two- and three-bond $^{13}C_\alpha$, $^2\Delta C_\alpha(N_iD)$ and $^3\Delta C_\alpha(N_{i+1}D)$, and three-bond $^{13}C_\beta$, $^3\Delta C_\beta(N_iD)$, isotope effects are practically the only useful reporters of the local geometry of the protein backbone.

The small magnitude of the majority of isotope effects considered here makes it necessary to reliably estimate random errors in the measurements and relate them to statistical deviations of the experimental shifts from the values predicted via empirical Karplus-type relationships. For the combined datasets of three- and two-bond isotope effects on $^{13}C_\alpha$ and $^{13}C_\beta$ backbone nuclei in ubiquitin and GB1 the achieved r.m.s.d.'s between the measured and back-calculated shifts (3.6, 4.6 and 7.2 ppb for $^3\Delta C_\alpha(N_{i+1}D)$, $^2\Delta C_\alpha(N_iD)$ and the subset of $^3\Delta C_\beta(N_iD)$ shifts, respectively) are about an order of magnitude lower than the corresponding ranges of shift variation (~45, ~40 and ~60 ppb for $^3\Delta C_\alpha(N_{i+1}D)$, $^2\Delta C_\alpha(N_iD)$ and the analyzed subset of $^3\Delta C_\beta(N_iD)$ shifts, respectively). The respective pair-wise r.m.s.d. between the shifts obtained in duplicate experiments are 2.5 and 2.9 ppb for the $^3\Delta C_\alpha(N_{i+1}D)$ and $^2\Delta C_\alpha(N_iD)$ shifts, and 8.3 ppb between

the $^{3}\Delta C_{\beta}(N_iD)$ shifts measured by the scheme of Fig. 1 and the 3D HACBN(H/D) experiments. In the case of $^{3}\Delta C_{\beta}(N_iD)$ shifts, lower accuracy of the measurements does not allow us to rule out that experimental errors are the primary source of the scatter in Fig. 8b. However, the errors in $^{2,3}\Delta C_{\alpha}$ shifts cannot explain the discrepancies between the measured and predicted isotope effects in Fig. 5. Therefore, other factors affecting deuterium isotope shifts must be in play beyond those described by empirical relationships in Eqs. 4–5 including: (1) dependence of isotope shifts on the amino-acid type, which was clearly demonstrated recently by the isotope shift measurements in the intrinsically disordered protein α-synuclein (Maltsev et al. 2012), (2) conformations of adjacent residues, (3) effects of hydrogen bonds involving amide protons, and (4) 'through-space' interactions with other nuclei in the protein structure. Although all these effects contribute to the net differences in shielding between the protonated and deuterated species, the main determinants of their absolute and relative magnitudes remain poorly understood. Nevertheless, the described approach provides a convenient means for the measurement of all one- to four-bond backbone and $^{13}C_{\beta}$ isotope shifts in a protein using a single experimental scheme.

Acknowledgments The authors thank Dr. Chenyun Guo for preparation of [U–^{15}N; ^{13}C]-labeled GB1, and Anna Krejčirikova (University of Maryland) for preparation of [U–^{15}N; ^{13}C]-labeled ubiquitin.

References

Abildgaard J, Hansen PE, Manalo MN, LiWang A (2009) Deuterium isotope effects on ^{15}N backbone chemical shifts in proteins. J Biomol NMR 44:119–126

Alexeev D, Bury SM, Turner MA, Ogunjobi OM, Muir TW, Ramage R, Sawyer L (1994) Synthetic, structural and biological studies of the ubiquitin system: chemically synthesized and native ubiquitin fold into identical three-dimensional structures. Biochem J 299:159–163

Anet FAL, Dekmezian AH (1979) Intrinsic steric deuterium isotope effects on proton and carbon-13 chemical shifts. J Am Chem Soc 101:5449–5451

Aydin R, Günther H (1981) Secondary deuterium/hydrogen isotope effects on carbon-13 chemical shifts in cycloalkanes. Downfield shifts over three and four bonds. J Am Chem Soc 103:1301–1303

Boyd J, Soffe N (1989) Selective excitation by pulse shaping combined with phase modulation. J Magn Reson 85:406–413

Briand J, Sørensen OW (1997) A novel pulse sequence element for biselective and independent rotations with arbitrary flip angles and phases for I and I{S} spin systems. J Magn Reson 125:202–206

Delaglio F, Grzesiek S, Vuister GW, Zhu G, Pfeifer J, Bax A (1995) NMRPipe: a multidimensional spectral processing system based on UNIX pipes. J Biomol NMR 6:277–293

Dunbrack RL (2002) Rotamer libraries in the 21st century. Curr Opin Struct Biol 12:431–440

Ernst L, Eltamany S, Hopf H (1982) Deuterium isotope effects on carbon-13 chemical shifts in cyclophanes. Deshielding intrinsic through-space and through-bond effects. J Am Chem Soc 104:299–300

Feeney J, Partington P, Roberts GCK (1974) The assignment of carbon-13 resonances from carbonyl groups in peptides. J Magn Reson 13:268–274

Frericks-Schmidt HL, Sperling LJ, Gao YG, Wylie BJ, Boettcher JM, Wilson SR, Rienstra CM (2007) Crystal polymorphism of protein GB1 examined by solid-state NMR spectroscopy and X-ray diffraction. J Phys Chem B 111:14362–14369

Gallagher T, Alexander P, Bryan P, Gilliland GL (1994) Two crystal structures of the B1 immunoglobulin-binding domain of streptococcal protein G and comparison with NMR. Biochemistry 33:4721–4729

Garbow JR, Weitekamp DP, Pines A (1982) Bilinear rotation decoupling of homonuclear scalar interactions. Chem Phys Lett 93:504–515

Gardner KH, Kay LE (1998) The use of ^{2}H, ^{13}C, ^{15}N multidimensional NMR to study the structure and dynamics of proteins. Annu Rev Biophys Biomol Struct 27:357–406

Gardner KH, Rosen MK, Kay LE (1997) Global folds of highly deuterated, methyl protonated proteins by multidimensional NMR. Biochemistry 36:1389–1401

Garrett D, Seok YJ, Peterkofsky A, Clore GM, Gronenborn AM (1997) Identification by NMR of the binding surface for the histidine-containing phosphocarrier protein HPr on the N-terminal domain of enzyme I of the *Escherichia coli* phosphotransferase system. Biochemistry 36:4393–4398

Geen H, Freeman R (1991) Band-selective radiofrequency pulses. J Magn Reson 93:93–141

Hansen PE (1983) Isotope effects on nuclear shielding. Ann Rep NMR Spectrosc 15:105–234

Hansen PE (1988) Isotope effects in nuclear shielding. Prog NMR Spectrosc 20:207–255

Hansen PE (2000) Isotope effects on chemical shifts of proteins and peptides. Magn Reson Chem 38:1–10

Hawkes GE, Randall EW, Hall WE, Gattegno D, Conti F (1978) Qualitative aspects of hydrogen-deuterium exchange in the proton, carbon-13, and nitrogen-15 nuclear magnetic resonance spectra of viomycin in aqueous solution. Biochemistry 17:3986–3992

Henry GD, Weiner JH, Sykes BD (1987) Backbone dynamics of a model membrane protein: measurement of individual amide hydrogen-exchange rates in detergent-solubilized M13 coat protein using ^{13}C NMR hydrogen/deuterium isotope shifts. Biochemistry 26:3626–3634

Jameson CJ (1996) Isotope effects on chemical shifts and coupling constants. In: Grant DM, Harris RK (eds) Encyclopedia of nuclear magnetic resonance. Wiley, New-York, NY, pp 2638–2655

Jaravine VA, Cordier F, Grzesiek S (2004) Quantification of H/D isotope effects on protein hydrogen-bonds by $^{h3}J_{NC'}$ and $^{1}J_{NC'}$ couplings and peptide group ^{15}N and ^{13}C′ chemical shifts. J Biomol NMR 29:309–318

Kainosho M, Nagao H, Tsuji T (1987) Local structural features around the C-terminal segment of *Streptomyces subtilisin* inhibitor studied by carbonyl carbon nuclear magnetic resonances of three phenylalanyl residues. Biochemistry 26: 1068–1075

Kay LE, Ikura M, Tschudin R, Bax A (1990) Three-dimensional triple-resonance NMR spectroscopy of isotopically enriched proteins. J Magn Reson 89:496–514

Kehl C, Simms AM, Toofanny RD, Daggett V (2008) Dynameomics: a multi-dimensional analysis-optimized database for dynamic protein data. Protein Eng Des Sel 21:379–386

LeMaster DM, LaIuppa JC, Kushlan DM (1994) Differential deuterium isotope shifts and one-bond 1H–13C scalar couplings in the conformational analysis of protein glycine residues. J Biomol NMR 4:863–870

Liu A, Wang J, Lu Z, Yao L, Li Y, Yan H (2008) Hydrogen-bond detection, configuration assignment and rotamer correction of side-chain amides in large proteins by NMR spectroscopy through protium/deuterium isotope efffects. ChemBioChem 9:2860–2871

LiWang AC, Bax A (1996) Equilibrium protium/deuterium fractionation of backbone amides in U – $^{13}C/^{15}N$ labeled human ubiquitin by triple resonance NMR. J Am Chem Soc 118: 12864–12865

Lovell SC, Word JM, Richardson JS, Richardson DC (2000) The penultimate rotamer library. Proteins 40:389–408

Majerski Z, Zuanic M, Metelko B (1985) Deuterium isotope effects on carbon-13 chemical shifts of protoadamantane. Evidence for geometrical dependence of $^{3}\Delta$ and $^{4}\Delta$ effects. J Am Chem Soc 107:1721–1726

Maltsev AS, Ying J, Bax A (2012) Deuterium isotope shifts for backbone ^{1}H, ^{15}N and ^{13}C nuclei in intrinsically disordered protein α-synuclein. J Biomol NMR 54:181–191

Marion D, Ikura M, Tschudin R, Bax A (1989) Rapid recording of 2D NMR spectra without phase cycling. Application to the study of hydrogen exchange in proteins. J Magn Reson 85:393–399

Meissner A, Sørensen OW (1998) New multidimensional editing experiments for measurement of amide deuterium isotope effects on C_β chemical shifts in [^{13}C, ^{15}N]-labeled proteins. J Magn Reson 135:547–550

Meissner A, Briand J, Sørensen OW (1998) Editing of multidimensional NMR spectra of partially deuterated proteins. Measurement of amide deuterium isotope effects on the chemical shifts of protein backbone nuclei. J Biomol NMR 12:339–343

Otter A, Liu X, Kotovych G (1990) Hydrogen-deuterium isotope effects in ^{13}C NMR experiments of peptides. J Magn Reson 86:657–662

Ottiger M, Bax A (1997) An empirical correlation between amide deuterium isotope effects on $^{13}C_\alpha$ chemical shifts and protein backbone conformation. J Am Chem Soc 119:8070–8075

Patt SL (1992) Single- and multiple-frequency-shifted laminar pulses. J Magn Reson 96:94–102

Ramage R, Green J, Muir TW, Ogunjobi OM, Love S, Shaw K (1994) Synthetic, structural and biological studies of the ubiquitin system: the total chemical synthesis of ubiquitin. Biochem J 299:151–158

Reuben J (1985) Isotopic multiplets in the carbon-13 NMR spectra of polyols with partially deuterated hydroxyls. 4. Molecular structure as reflected in the carbon-13 NMR spectra of oligosaccharides with partially deuterated hydroxyls. J Am Chem Soc 107:1747–1755

Scouras AD, Daggett V (2011) The dynameomics rotamer library: amino acid side chain conformations and dynamics from comprehensive molecular dynamics simulations in water. Protein Sci 20:341–352

Shaka AJ, Keeler J, Frenkiel T, Freeman R (1983) An improved sequence for broadband decoupling: WALTZ-16. J Magn Reson 52:335–338

Shaka AJ, Lee CJ, Pines A (1988) Iterative schemes for bilinear operators; application to spin decoupling. J Magn Reson 77:274–293

Sheppard D, Guo C, Tugarinov V (2009a) 4D 1H–13C NMR spectroscopy for assignments of alanine methyls in large and complex protein structures. J Am Chem Soc 131:1364–1365

Sheppard D, Guo C, Tugarinov V (2009b) Methyl-detected 'out-and-back' NMR experiments for simultaneous assignments of Alaβ and Ileγ2 methyl groups in large proteins. J Biomol NMR 43:229–238

Sheppard D, Li DW, Brüschweiler R, Tugarinov V (2009c) Deuterium spin probes of backbone order in proteins: a ^{2}H NMR relaxation study of deuterated carbon-α sites. J Am Chem Soc 131:15853–15865

Sun H, Tugarinov V (2012) Precision measurements of deuterium isotope effects on the chemical shifts of backbone nuclei in proteins: correlations with secondary structure. J Phys Chem B 116:7436–7448

Sun H, Long D, Brüschweiler R, Tugarinov V (2013) Carbon Relaxation in $^{13}C_\alpha$-H_α and $^{13}C_\alpha$-D_α spin pairs as a probe of backbone dynamics in proteins. J Phys Chem B 117:1308–1320

Takeda M, Jee J, Ono AM, Terauchi T, Kainosho M (2009) Hydrogen exchange rate of tyrosine hydroxyl groups in proteins as studied by the deuterium isotope effect on C_ζ chemical shifts. J Am Chem Soc 131:18556–18562

Takeda M, Jee J, Terauchi T, Kainosho M (2010) Detection of the sulfhydryl groups in proteins with slow hydrogen exchange rates and determination of their proton/deuteron fractionation factors using the deuterium-induced effects on the $^{13}C_\beta$ NMR signals. J Am Chem Soc 132:6254–6260

Tomlinson JH, Ullah S, Hansen PE, Williamson MP (2009) Characterization of salt bridges to lysines in the protein G B1 domain. J Am Chem Soc 131:4674–4684

Tüchsen E, Hansen PE (1991) Hydrogen bonding monitored by deuterium isotope effects on carbonyl ^{13}C chemical shift in BPTI: intra-residue hydrogen bonds in antiparallel β-sheet. Int J Biol Macromol 13:2–8

Van der Kamp MW, Schaeffer RD, Jonsson AL, Scouras AD, Simms AM, Toofanny RD, Benson NC, Anderson PC, Merkley ED, Rysavy S, Bromley D, Beck DAC, Daggett V (2010) Dynameomics: a comprehensive database of protein dynamics. Structure 18:423–435

Venters RA, Farmer BT, Fierke CA, Spicer LD (1996) Characterizing the use of perdeuteration in NMR Studies of large proteins: ^{13}C, ^{15}N and ^{1}H assignments of human carbonic anhydrase II. J Mol Biol 264:1101–1116

Vijay-Kumar S, Bugg CE, Cook WJ (1987) Structure of ubiquitin refined at 1.8 angströms resolution. J Mol Biol 194:531–544

Zhu G, Bax A (1990) Improved linear prediction for truncated signals of known phase. J Magn Reson 90:405–410

Zhu G, Bax A (1992) Two-dimensional linear prediction for signals truncated in both dimensions. J Magn Reson 98:192–199